LA-UR-24-32825

Approved for public release; distribution is unlimited.

Title:	Modeling partial reflection paths for infrasound analysis
Author(s):	Blom, Philip Stephen
Intended for:	Report
Issued:	2024-12-04

Modeling Partial Reflection Paths for Infrasound Analysis

Philip Blom

December 2, 2024

Summary

Numerical methods enabling simulation of scattered and partially reflected infrasonic propagation paths produced by interaction with fine-scale structure in the middle atmosphere have been implemented in the *infraGA* ray tracing software. This capability enables simulation of ensonification in the classical stratospheric "shadow zone" that has been observed during the Humming Roadrunner and LSECE surface explosion campaigns as well as in other data sets. In the case of LSECE, a pair of stations roughly 140 kilometers east of the source location observed arrivals with celerities (horizontal group velocities) slightly slower than observed stratospheric paths at similar azimuths. The arrivals exhibited increasing trace velocity later in the wavetrain indicating a steepening of the arrival path for longer or slower propagation paths. Simulation of partially reflected paths using the updated *infraGA* software methods finds good agreement between observed and predicted infrasonic ensonification at these locations within the stratospheric shadow zone. Further development of the partial reflection physics and comparison with other data sets is needed to more robustly understand how such anomalous infrasonic signals can be predicted; however, the demonstration of this capability is a promising first step in such analyses.

Anomalous Infrasonic Signals in the Stratospheric Shadow Zone

Infrasonic signals propagating through the lower-atmosphere are upwardly refracted due to the decreasing temperatures in the troposphere. In the absence of sufficiently strong tropospheric winds (i.e., jet stream), this upward refraction results in an acoustic "shadow zone" between the source and refracted arrivals from stratospheric winds and/or thermospheric temperature gradients which typically return to the ground at distances of 200 and 300 km, respectively. Anomalous ensonification within this "shadow zone" has been observed in a number of cases and such signals are typically attributed to scattering and partial reflections from fine-scale wind structures in the middle atmosphere. Analysis and modeling of such signals has been previously conducted and reported by Kulichkov *et al.* (2010), Ostashev *et al.* (2012), Green *et al.* (2018), Blixt *et al.* (2019), Blom (2023), and others.

Modeling the propagation of signals scattered or partially reflected by fine-scale structure is somewhat challenging as inclusion of such atmospheric structure requires higher spatial grid resolution and frequency considerations in finite-frequency simulations. Additionally, exactly how the fine-scale structure is defined can require stochastic analysis with multiple fine-scale structure instances considered and ensembles of simulation runs. Alternately, ray tracing methods can be used by defining a reflection altitude at which to impose a reflection and tracking how the ray path propagates following being reflected by wind shear at a given altitude. Such analysis was recently conducted as part of analysis of the Large Surface Explosion Coupling Experiment (LSECE) using a relatively simplistic framework in which ray paths were computed out to a distance halfway between the source and station. Assuming ray paths were scattered from fine-scale structure at that point, the scattered or partially reflected path would arrive near the station. The up- and down-going legs of such propagation paths are symmetric so that the celerity at the mid-point (the ratio of the horizontal range and travel time) is the same as that at the arrival location. Both the range and travel time double, so the ratio remains the same. Visualization of this analysis is shown in Fig. 1 for a pair of stations located approximately 140 km east of the surface explosion location.

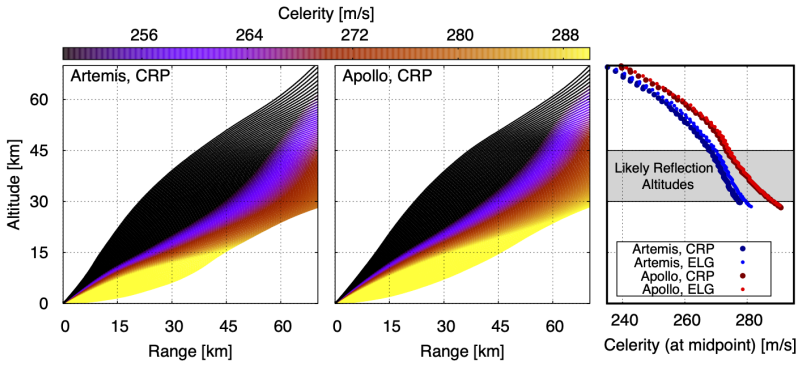

Figure 1: Simulation of scattered arrivals via ray tracing to the mid-point between source and station for the LSECE surface explosions. See Blom (2023) for full discussion.

The observed infrasonic signals in the shadow zone during the LSECE explosions are shown in Fig. 2. These stations were located within the classical stratospheric shadow zone and, therefore, not expected to detect signal from the surface explosions; however, coherent infrasonic signals were detected on both stations for both events with celerities on the order of 270 – 290 m/s. Stations further to the east detected signals from the explosions with celerities on the order of 290 – 310 m/s consistent with stratospheric propagation paths, so these arrivals are likely through a distinct propagate waveguide. The trace velocity (related to the inclination angle of the planewave estimate across the station elements) increases later in the wavetrain, indicating that later arriving energy has steeper inclination angle at the station.

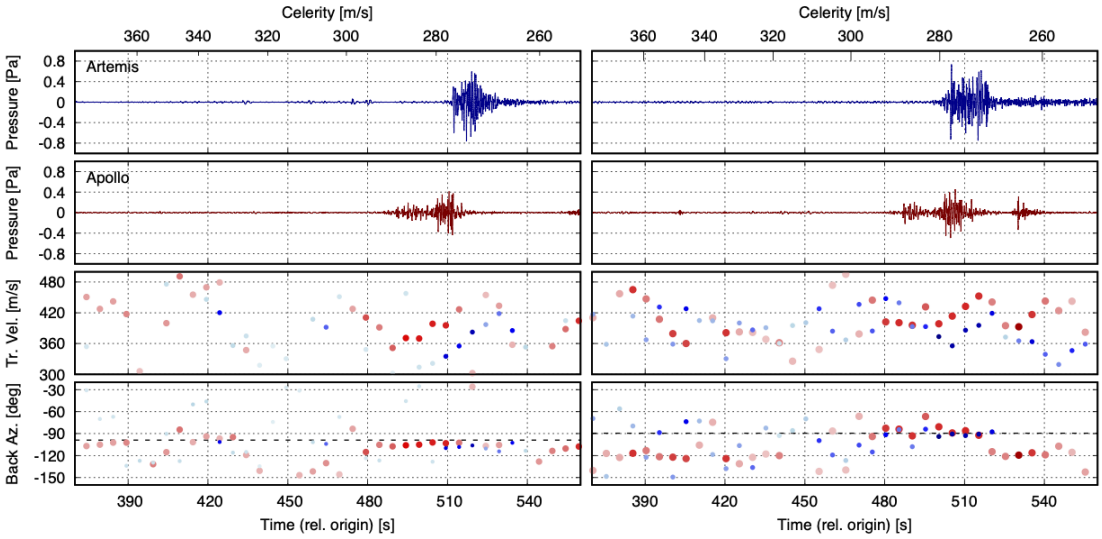

Figure 2: Infrasonic signatures at ELG (left) and CRP (right) stations for the LSECE surface explosions. Arrivals are slightly slower than stratospheric arrivals osberved on other stations (290 - 310 m/s) and exhibit increasing trace velocity later in the wavetrain typical of scattered and partially reflected arrivals seen in other analyses.

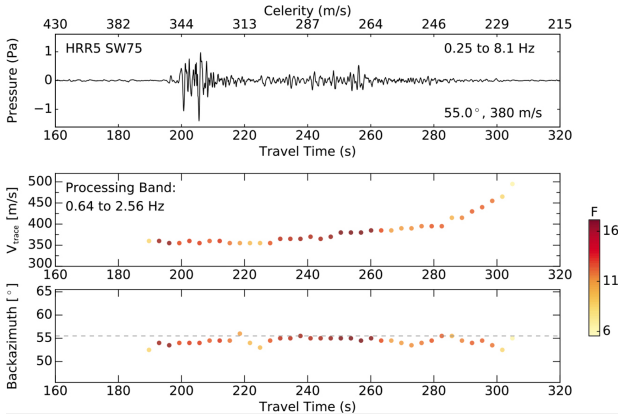

Figure 3: Infrasonic signal in the stratospheric "shadow zone" observed during the Humming Roadrunner surface explosion series. The station is roughly 75 km southwest of the explosive source location. The infrasonic wavetrain lasts more than 100 seconds and exhibits increasing trace velocity later in time. Figure from Green *et al.* (2018).

Similar observations have been documented for other surface explosions and impulsive sources (see Kulichkov *et al.*, 2010; Ostashev *et al.*, 2012; Green *et al.*, 2018; Blixt *et al.*, 2019). An example shadow zone detection observed by Green *et al.* (2018) during the Humming Roadrunner experiment is shown in Fig. 3. This stations is located nearer to the source (75 km compared to 140 km for the LSECE data). The range of trace velocities observed in this arrival is similar to those during LSECE; however, the celerity and duration cover a notably larger range. The scattered arrival at HRR lasts more than 100 seconds and extends from 240 - 340 m/s celerity while those during LSECE were 15 - 30 seconds and limited to 270 - 290 m/s celerity. This is likely due to the difference in source-receiver range, but also to the difference in source energy (HRR5 was a 45-ton equivalent TNT surface explosion, while both LSECE explosions were 1-ton equivalent TNT).

Modeling Partially Scattered Paths - Ray Tracing

Numerical simulations of scattering and partial reflections from fine-scale structure in the atmosphere can be challenging as finite-frequency simulations require significantly higher spatial and temporal resolution to include such atmospheric variations in the propagation medium description and to accurately capture the physics of acoustic waves interacting with fine-scale structures in the

atmosphere. A more numerically efficient framework for modeling such propagation paths can be constructed by imposing a reflection condition at some altitude in the atmosphere in ray tracing simulations. Such a condition is straightforward to implement in an effective sound speed framework as the ambient winds are included in the sound speed definition using such an approximation.

Effective Sound Speed Approximation

In the effective sound speed approximation (Godin, 2002), the ambient winds are projected onto the sound speed as, $c_{\text{eff}}(z) = c_0(z) + \hat{e}_\varphi \cdot \vec{v}_0(z)$ where c_0 denotes the adiabatic sound speed, $\vec{v}_0$ denotes the ambient winds, and $\hat{e}_\varphi$ is the azimuthal unit vector denoting the direction of propagation in the horizontal plane. In most applications, the atmosphere is assumed to be stratified (only dependent on the altitude, z); however, range dependence can be included relatively easily. For this initial analysis, the effective sound speed approximation is applied to avoid the need to include the atmospheric winds in the reflection conditions.

An optional configuration flag has been included in the *infraGA* ray tracing software to impose reflection of ray paths from a user specified altitude. This parameter is referenced by `refl_alt` and can be referenced in the C/C++ methods as,

```
infraga-2d -prop ToyAtmo.met azimuth=90.0 refl_alt=35
```

In the Python wrappers for *infraGA* this is similar referenced,

```
infraga 2d prop --atmo-file ToyAtmo.met --azimuth 90.0 --refl-alt 35
```

where the value specified in in kilometers above sea level (G2S altitudes are similar defined as relative to sea level).

An example set of ray paths using a reflection altitude of 35 kilometers is shown in Fig. 4. In the figure, the inner edge of stratospheric ensonification region can be observed at roughly 155 km range. These ray paths have turning heights near 30 kilometers, so they don't reach the imposed reflection altitude. For steeper inclination ray paths, the energy isn't captured in the stratospheric waveguide and reaches the imposed reflection height where they are turned back towards the ground surface. This produces a line of arrival points in the lower panel of the figure between 35 and the inner edge of the stratospheric ensonification zone. inclination angles in this simulation were limited to 60°, but if this limit were increased then overly steep paths may be reflected back nearer to the source, but for this analysis where stations are further downrange these steep paths are not relevant and not included in simulations.

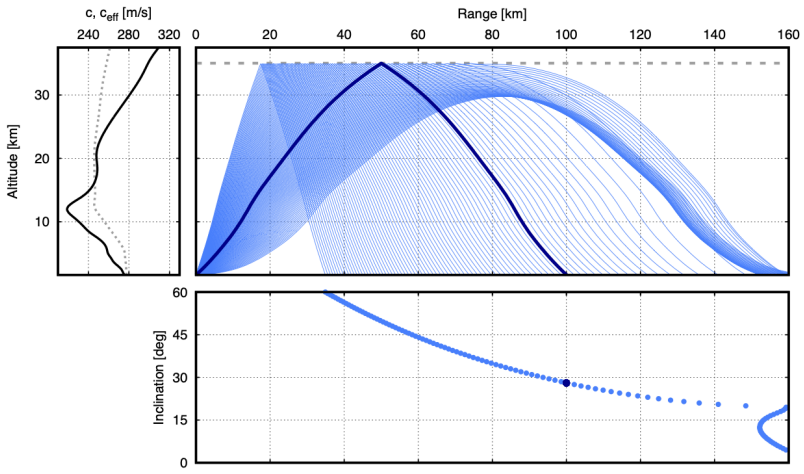

Figure 4: Propagation paths with an imposed reflection altitude of 35 kilometers. Ray paths with turning heights below this altitude propagate as normal, but steeped angled paths are reflected by the software when they reach this altitude producing ensonification in the stratospheric shadow zone. The darker blue path shows the path that arrives at 100 km downrange for this reflection altitude.

Moving Medium Considerations

Application of Hamilton-Jacobi dynamic relations to the acoustic Eikonal equation leads to the governing equations for acoustic ray tracing,

$$\frac{\partial \vec{x}}{\partial s} = \frac{\vec{c}_g}{c_g}, \qquad \vec{c}_g = c\frac{\vec{\psi}}{\psi} + \vec{v}, \tag{1a}$$

$$\frac{\partial \psi_j}{\partial s} = -\frac{1}{c_g}\left(\psi \frac{\partial c}{\partial x_j} + \vec{\psi}\cdot\frac{\partial \vec{v}}{\partial x_j}\right), \tag{1b}$$

where $\vec{x}$ and $\vec{\psi}$ are the position and EIkonal (momentum) vectors, respectively, c and v are the sound speed and ambient winds, respectively, and $\vec{c}_g$ denotes the group velocity. In the effective sound speed approximation this reduces to a simpler pair of relations,

$$\frac{\partial \vec{x}}{\partial s} = \frac{\vec{\psi}}{\psi}, \qquad \frac{\partial \vec{\psi}}{\partial s} = -\frac{\psi}{c_{\text{eff}}}\vec{\nabla} c_{\text{eff}}. \tag{2}$$

The reflection condition used to continue ray tracing once a path intercepts the ground surface have been derived in the limiting case that the wind is zero at the ground surface (see Blom & Waxler, 2017). This leads to reflection conditions for the ray tracing and auxiliary parameters of the form,

$$\begin{pmatrix} x\left(s_0+0^+,\theta,\phi\right) \\ y\left(s_0+0^+,\theta,\phi\right) \\ z\left(s_0+0^+,\theta,\phi\right) \end{pmatrix} = \begin{pmatrix} x_0\left(\theta,\phi\right) \\ y_0\left(\theta,\phi\right) \\ z_0\left(\theta,\phi\right) \end{pmatrix}, \qquad \begin{pmatrix} \psi_x\left(s_0+0^+,\theta,\phi\right) \\ \psi_y\left(s_0+0^+,\theta,\phi\right) \\ \psi_z\left(s_0+0^+,\theta,\phi\right) \end{pmatrix} = \begin{pmatrix} \psi_{x,0}\left(\theta,\phi\right) \\ \psi_{y,0}\left(\theta,\phi\right) \\ -\psi_{z,0}\left(\theta,\phi\right) \end{pmatrix}, \tag{3a}$$

$$\begin{pmatrix} \mathcal{X}^{(\theta)}\left(s_0+0^+,\theta,\phi\right) \\ \mathcal{Y}^{(\theta)}\left(s_0+0^+,\theta,\phi\right) \\ \mathcal{Z}^{(\theta)}\left(s_0+0^+,\theta,\phi\right) \end{pmatrix} = \begin{pmatrix} \mathcal{X}_0^{(\theta)}\left(\theta,\phi\right) \\ \mathcal{Y}_0^{(\theta)}\left(\theta,\phi\right) \\ -\mathcal{Z}_0^{(\theta)}\left(\theta,\phi\right) \end{pmatrix} \tag{3b}$$

$$\begin{pmatrix} \Psi_x^{(\theta)}\left(s_0+0^+,\theta,\phi\right) \\ \Psi_y^{(\theta)}\left(s_0+0^+,\theta,\phi\right) \\ \Psi_z^{(\theta)}\left(s_0+0^+,\theta,\phi\right) \end{pmatrix} = \begin{pmatrix} \Psi_{x,0}^{(\theta)}\left(\theta,\phi\right) \\ \Psi_{y,0}^{(\theta)}\left(\theta,\phi\right) \\ -\Psi_{z,0}^{(\theta)}\left(\theta,\phi\right) - \frac{2}{c_0}\left(\frac{c_{\text{src}}}{c_0}\frac{\partial c_0}{\partial z} + \vec{\psi}_0\cdot\frac{\partial \vec{v}_0}{\partial z}\right)\frac{c_{\text{src}}}{c_0}\frac{\mathcal{Z}_0^{(\theta)}}{\psi_{z,0}} \end{pmatrix}. \tag{3c}$$

The normal Eikonal and spatial auxiliary parameter components change sign in reflection; however, the normal auxiliary Eikonal picks up additional terms due to the sound speed and wind gradients near the ground. In the case that wind is included in these reflection conditions, the various terms will pick up additional terms due to the moving propagation medium. Additional study of the ray tracing equations and how reflection conditions can be generalized to include ambient winds at the reflection location are needed for a full 3D simulation capability.

Comparison for LSECE Surface Explosions

The imposed reflection altitude condition demonstrated in Fig. 4 includes only a single reflection altitude and is not immediately useful in predicting the combination of all energy possibly incident at a given location. A pseudo-eigenray method can be constructed by considering the arrival range of the ray paths as a function of inclination and imposed reflection altitude, $r_0\left(\vartheta, z_{\text{refl}}\right)$. In the effective

sound speed limit, this is a uni-variate optmization (in 3D ray tracing, the arrival is characterized by $x_0(\vartheta, z_{\text{refl}})$ and $y_0(\vartheta, z_{\text{refl}})$ and identifying specific source-receiver paths is more complicated). A method has been developed as a Python wrapped iteration of propagation simulations with varying `--refl-alt` to compute paths reflected from different atmospheric layers and identify those that arrive at a given station range. That is, it cycles through computations of r_0 and identifies those combinations of ϑ_k and $z_{\text{refl},k}$ which produces $r_0 = r_{\text{station}}$. This method can be accessed using,

```
infraga 2d refl_eigs --atmo-file ToyAtmo.met --rcvr-rng 140.0 --rcvr-az -90.0 \
                             --wvfrm-yield 1.0e3 --local-temp-dir refl_temp
```

Full usage info can be accessed as `infraga 2d refl_eigs -h`. As noted above, a maximum inclination of 60° was used in this analysis and the considered reflection layers cover altitudes between 25 and 45 kilometers. The default values of these various parameters are still being determined.

An example result from the `refl_eigs` method is shown in Fig 5 for the ELG station deployed during the LSECE. This station was roughly 140 kilometers east of the source and observed signals as shown in Fig. 2. Scattered propagation paths arriving near the ELG station were identified using the above method and reflection altitudes between 30 and 40 are found to dominate the scattered energy in relatively good agreement with the preliminary analysis summarized in Fig. 1 (in that analysis, the scattering altitude extended further to 45 kilometers altitude). The waveform predicted here used a 1-ton equivalent TNT explosion blastwave and weakly non-linear impulse propagation as summarized in Blom & Waxler (2021). The constructive and deconstructive interference between the individual arrivals produces a complex waveform in this case; though, this is somewhat dependent on the resolution of reflection layers (set to 500 meters in this analysis). Also, it should be noted that in this current formulation, the reflection coefficient is assumed to be unity in these simulations so that the predicted amplitude is an overestimate. Further analysis considering the impact of varying the scattering altitude resolution and reflection/transmission coefficients is needed to identify how much energy is actually scattered by the wind shear and fine-scale structure in the atmosphere.

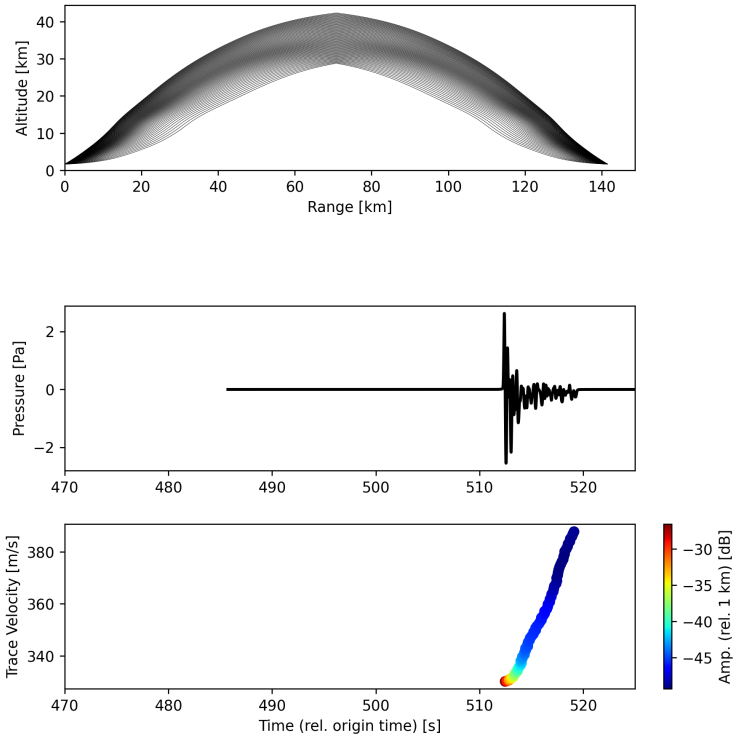

Figure 5: Predicted scattered arrivals at ELG using the user imposed reflection altitude introduced in *infraGA*. Paths reflecting from wind shear and fine-scale structure between 30 and 40 kilometers are expected to ensonify the station and the trace velocity is expected to increase later into the wavetrain as observed in Fig. 2.

The predicted partially reflected arrivals for both LSECE events (Artemis and Apollo) at the ELG and CRP stations (left and right columns, respectively) are shown in Fig. 6. The general trends observed in Fig 2 are reproduced in these predictions with the signals during the Artemis

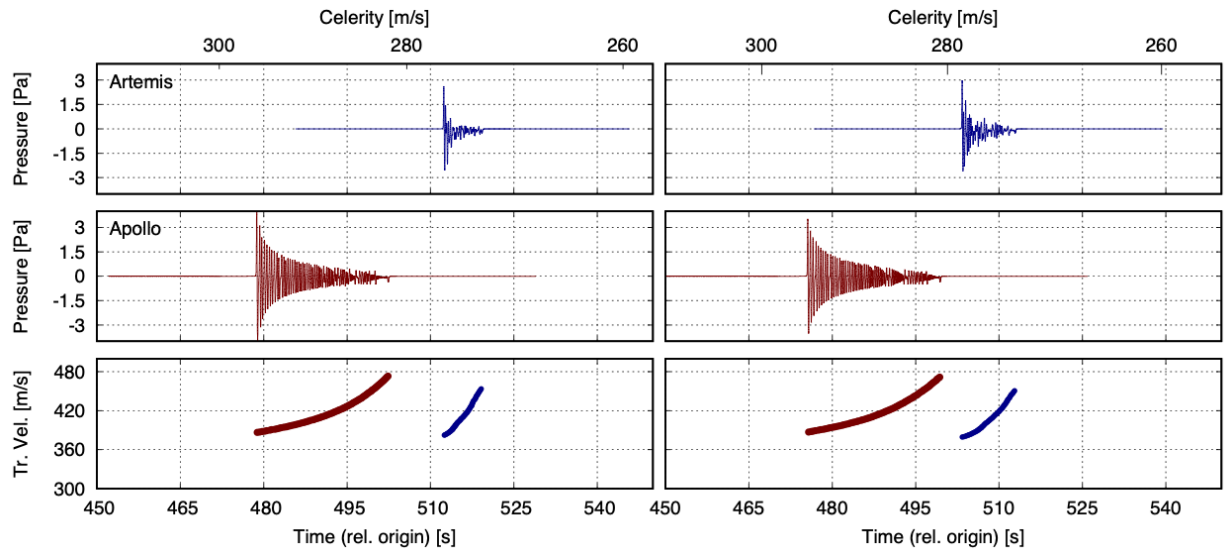

Figure 6: Predicted partially reflected arrival wavetrains for the LSECE events at the ELG and CRP stations (left and right, respectively). General trends between the two events (Artemis signals arriving later in time and being shorter duration) are in agreement with observations shown in Fig. 2.

event arriving later in time and being shorter duration. As indicated above, these simulations assumed possible scattering layers every 500 meters between 25 and 45 kilometers altitude. Whether wind shear or fine-scale structure was present at a given altitude in the atmosphere cannot be explicitly known, so that some comparison between observed and predicted arrival time and trace velocity is needed to identify those altitude from which energy was likely scattered. This and other analysis of these anomalous propagation paths is enabled by the simulation capabilities documented here, and are planned for future R&D.

Conclusions

Ray-based simulation methods have been developed to predict infrasonic energy scattered and partially reflected from wind shear and fine-scale structure in the atmosphere by defining a reflecting layer at some altitude in the atmosphere. This method is used here to investigate the anomalous infrasonic signals observed at the ELG and CRP stations roughly 140 kilometers east of the LSECE surface explosions. At these stations, infrasonic signals exhibiting slightly sub-stratospheric celerities (270 - 290 m/s compared with 290 – 310 m/s for observations at other stations further to the east) were observed with trace velocities increasing later in the arrival wavetrain. Simulations produce predictions in general agreement with these characteristics and also show good agreement with other characteristics of the arrivals such as those during the Artemis event having longer propagation times and shorter durations than those during Apollo.

A more robust propagation modeling capability with paths extending into three dimensions is needed to avoid the simplifications of the effective sound speed approximation; though, such a capability will require mathematical and physical analysis to derive the generalized reflection conditions when ambient wind is non-zero. Continued use and analysis of this anomalous infrasound propagation modeling capability is needed and, fortunately, both existing data sets and data collection opportunities during future surface explosion campaigns are being identified.

References

- Blixt, E. M., Näsholm, S. P., Gibbons, S. J., Evers, L. G., Charlton-Perez, A. J., Orsolini, Y. J., & Kværna, T. (2019). "Estimating tropospheric and stratospheric winds using infrasound from explosions." *Journal of the Acoustical Society of America*, **146**(2), 973-982.

- Blom, P., & Waxler, R. (2012). "Impulse propagation in the nocturnal boundary layer: Analysis of the geometric component." *The Journal of the Acoustical Society of America*, 131(5), 3680-3690.

- Blom, P., & Waxler, R. (2017). "Modeling and observations of an elevated, moving infrasonic source: Eigenray methods." *The Journal of the Acoustical Society of America*, 141(4), 2681-2692.

- Blom, P., & Waxler, R. (2021). Characteristics of thermospheric infrasound predicted using ray tracing and weakly non-linear waveform analyses. *The Journal of the Acoustical Society of America*, 149(5), 3174-3188.

- Blom, P. (2023). "Regional infrasonic observations from surface explosions–influence of atmospheric variations and realistic terrain." *Geophysical Journal International*, 235(1), 200-215.

- Godin, O. A. (2002). "An effective quiescent medium for sound propagating through an inhomogeneous, moving fluid." *The Journal of the Acoustical Society of America*, 112(4), 1269-1275.

- Green, D. N., Waxler, R., Lalande, J. M., Velea, D., & Talmadge, C. (2018). "Regional infrasound generated by the Humming Roadrunner ground truth experiment." *Geophysical Journal International*, 214(3), 1847-1864.

- Kulichkov, S. N., Chunchuzov, I. P., & Popov, O. I. (2010). "Simulating the influence of an atmospheric fine inhomogeneous structure on long-range propagation of pulsed acoustic signals." *Izvestiya, Atmospheric and Oceanic Physics*, 46(1), 60-68.

- Ostashev, V. E., Chunchuzov, I. P., & Wilson, D. K. (2005). "Sound propagation through and scattering by internal gravity waves in a stably stratified atmosphere." *Journal of the Acoustical Society of America*, 118(6), 3420-3429.